

TURBULENT STRUCTURE OF A STRATIFIED SUPERNOVA-DRIVEN INTERSTELLAR MEDIUM

M. K. RYAN JOUNG^{1,2} AND MORDECAI-MARK MAC LOW^{1,2}

Draft version September 9, 2018

ABSTRACT

To study how supernova feedback structures the turbulent interstellar medium, we construct 3D models of vertically stratified gas stirred by discrete supernova explosions, including vertical gravitational field and parametrized heating and cooling. The models reproduce many observed characteristics of the Galaxy such as global circulation of gas (i.e., galactic fountain) and the existence of cold dense clouds in the galactic disk. Global quantities of the model such as warm and hot gas filling factors in the midplane, mass fraction of thermally unstable gas, and the averaged vertical density profile are compared directly with existing observations, and shown to be broadly consistent. We find that energy injection occurs over a broad range of scales. There is no single effective driving scale, unlike the usual assumption for idealized models of incompressible turbulence. However, >90% of the total kinetic energy is contained in wavelengths shortward of 200 pc. The shape of the kinetic energy spectrum differs substantially from that of the velocity power spectrum, which implies that the velocity structure varies with the gas density. Velocity structure functions demonstrate that the phenomenological theory proposed by Boldyrev is applicable to the medium. We show that it can be misleading to predict physical properties such as the stellar initial mass function based on numerical simulations that do not include self-gravity of the gas. Even if all the gas in turbulently Jeans unstable regions in our simulation is assumed to collapse and form stars in local freefall times, the resulting total collapse rate is significantly lower than the value consistent with the input supernova rate. Supernova-driven turbulence inhibits star formation globally rather than triggering it.

Subject headings: hydrodynamics — ISM: kinematics and dynamics — ISM: structure — methods: numerical — turbulence

1. INTRODUCTION

The interstellar medium (ISM) is observed to be turbulent. The electron density spectrum in the warm ionized medium shows a nearly Kolmogorov spectrum over at least six orders of magnitude in length (Armstrong et al. 1995). Supposing the small density perturbations measured to behave as a passive scalar, this can be taken as evidence for a Kolmogorov velocity spectrum in that gas. Giant molecular clouds, which contain most of the molecular gas, show supra-thermal emission linewidths (Zuckerman & Palmer 1974), indicating the presence of supersonic random motions.

What drives this turbulence? Massive stars are a major structuring agent in the ISM (McCray & Snow 1979). Once formed inside molecular clouds, they influence the surrounding medium via intense ionizing radiation and stellar winds until they end their lives in catastrophic explosions as supernovae, heating and stirring the ISM throughout their lives. Among these energetic processes, supernovae (and their collective effect, superbubbles) are likely to be the dominant contributor to the observed supersonic turbulence (Norman & Ferrara 1996; see Mac Low & Klessen 2004 for a recent review). This turbulence changes the balance between pressure and gravity on a wide range of scales, from galactic (Boulares & Cox 1990) to sub-cloud scales (e.g., Larson 1981), and in turn may regulate subsequent star formation, hence the term “feedback.” With strong enough feedback, a galactic-scale superwind may be driven out of the galaxy (Heckman et al. 2000, 2001).

Our understanding of how the radiative and hydrodynamic

feedback affects spatio-temporal structure of the ISM and star formation is only qualitative. It remains difficult to incorporate the feedback into a consistent theory of star formation and the ISM, partly because star formation is an inherently complex phenomenon that involves an interplay between gravity, magnetohydrodynamics, and thermodynamics of compressible gas. Yet it is a crucial physical process for correct predictions of, e.g., the thickness, disk stability, and star formation rate of galaxies. Many of the serious problems that cosmological models are faced with today are also believed to be associated with such feedback.³

Since no analytic theory based on first principles exists for turbulence in a compressible medium (see, however, a heuristic model by Sasao 1973), most previous work has relied heavily on numerical methods. Recent numerical simulations in periodic boxes yielded key insights into the role of turbulence in star formation. First, supersonic turbulence in an isothermal or an adiabatic medium was found to decay quickly, i.e. within a sound crossing time, whether the medium was magnetized or not (Stone et al. 1998; Mac Low et al. 1998; Padoan & Nordlund 1999), unless it was constantly stirred by an external source of driving (Mac Low 1999). Second, supersonic turbulence delays or sometimes prevents collapse (Klessen et al. 2000, hereafter KHM00), and is hence thought to be responsible for the observed low overall star formation efficiencies (Vázquez-Semadeni et al. 2005). Overall, turbulence impedes collapse in unstable regions. Third, in contrast to the second point, it also creates

¹ Department of Astronomy, Columbia University, 550 West 120th Street, New York, NY 10027; moo@astro.columbia.edu

² Department of Astrophysics, American Museum of Natural History, 79th Street at Central Park West, New York, NY 10024; mordecai@amnh.org

³ The standard CDM paradigm predicts basic properties of the luminous component of matter on galactic and sub-galactic scales which are seriously inconsistent with observations. Outstanding astrophysical problems include incorrect predictions for the shape of the galaxy luminosity function and for the fraction of gas that should have cooled to form galaxies (the overcooling problem) (Somerville & Primack 1999; Cole et al. 2000).

converging flows that may enhance density and thus promote collapse (Ballesteros-Paredes et al. 1999). Even when turbulence can support a cloud globally against gravitational collapse, it produces density enhancements that allow local collapse in both non-magnetized (KHM00) and magnetized media (Heitsch, Mac Low, & Klessen 2001, hereafter HMK01). However, the net effect of turbulence is to inhibit collapse (Mac Low & Klessen 2004).

In some of these previous simulations, turbulence was seeded as the initial condition and left to decay for the rest of the run (Porter et al. 1992; Porter et al. 1998; Stone et al. 1998; Mac Low et al. 1998; Padoan & Nordlund 1999). In other simulations, turbulence was driven constantly but the driving was included only in a general way as ubiquitous Fourier forcing, i.e., a random forcing in a prescribed narrow range of wavenumbers applied uniformly to the box (Mac Low 1999; KHM00; HMK01). These models only partly represent the real ISM, where forced and decaying regimes may coexist (Avila-Reese & Vázquez-Semadeni 2001) and where an appropriate forcing function is probably broad-band (Norman & Ferrara 1996). It has been demonstrated that the slope of the power spectrum for the forcing function profoundly affects the statistics of turbulent fluctuations (Bonazzola et al. 1987; Vázquez-Semadeni & Gazol 1995; Biferale et al. 2004). Hence, it is of great interest to determine the wavelength distribution of the kinetic energy in a more realistic medium driven by *discrete physical space forcing*.

Our goal is to examine physical characteristics of the ISM driven by realistic, discrete physical space forcing in 3D. In particular, we study density and velocity structures and determine the kinetic energy power spectrum. If, as some previous works suggest, the interaction of blast waves from supernovae structures the interstellar gas, we must resolve the individual explosions in order to correctly reproduce the main statistical properties of the ISM. For an accurate simulation of supernova driving, a wide range of length scales from small clouds (~ 1 pc) to at least the “driving scale” (using the language derived from incompressible turbulence research) must be resolved. In addition, to predict the cloud structure, the model must take into account appropriate heating and radiative cooling processes.

There have been modeling efforts toward more realistic supernova driving by including its explosive nature. Rosen, Bregman, & Norman (1993), Rosen & Bregman (1995), and Wada & Norman (2001) performed two-dimensional hydrodynamic simulations for the ISM in a galactic disk including feedback from supernovae and/or stellar winds. Results from two-dimensional models must be interpreted with caution, since turbulence behaves differently in 2D than in 3D: in 2D, an inverse cascade of energy occurs towards large scales, while the enstrophy, the square of vorticity, cascades to small scales (Kraichnan 1967; Frisch 1995). More recently, three-dimensional models have been studied by several groups. These authors find that blast waves from supernovae sweep up the ISM into relatively thin shells that collide with one another to form cold dense clouds. However, none of the goals raised above has been adequately addressed. Korpi et al. (1999) used resolution of 10 pc, insufficient to follow the details of turbulent interactions, and only covered $(0.5 \text{ kpc})^2 \times 2 \text{ kpc}$, although they did include magnetic field and galactic shear. Their main interest was to simulate a turbulent galactic dynamo. Slyz et al. (2005) included self-gravity of the gas but suffer from low spatial resolution (≥ 10 pc) and the absence of vertical density stratification. Kim et al. (2001) and Mac Low

et al. (2005) also included magnetic field, but not galactic stratification. Avillez (2000) and Avillez & Berry (2001) used a stratified model similar to ours, but their studies focused on the properties of a Galactic fountain in the Milky Way. All the aforementioned 3D models employed minimum gas temperatures $T_{min} = 100\text{--}310$ K, so no cold gas could form. The difference between Avillez & Breitschwerdt (2004a, b) and the present work is more subtle, and will be discussed in § 3.2.

We simulate a small patch of our Galaxy, $(0.5 \text{ kpc})^2$ in area. The computation box is elongated in z and extends from -5 kpc to $+5$ kpc to study the vertical structure. We choose the length scales in our simulations ($2 \text{ pc} \leq l \leq 10 \text{ kpc}$) to lie between those of star-forming molecular clouds and those of large-scale galactic outflows (Heckman et al. 2000, 2001). Our box size represents an optimal choice to improve our understanding of this enigmatic yet relatively unexplored regime. Expanding shells and their interactions are well-resolved at this scale. We attempt to build local, high-resolution models of the ISM based on which subgrid models for turbulent pressure can be developed, that will provide insight into how supernova feedback should be treated in global, cosmological simulations. We will continue to pursue this problem in a companion paper (M. Joung & M. Mac Low 2005, in preparation; hereafter Paper II). Here, in Paper I, we describe our numerical model (§ 2) and present the basic results (§ 3). In § 4, we explore where gravitational collapse would occur in the presence of explosion-driven turbulence. Finally, we summarize our findings and discuss their implications in § 5.

2. THE MODEL

2.1. Basic Features

Our simulations are performed using Flash (Fryxell et al. 2000), an Eulerian astrophysical hydrodynamics code with adaptive mesh refinement (AMR) capability, developed by the Flash Center at the University of Chicago. It solves the Euler equations using the piecewise-parabolic method (Colella & Woodward 1984) to handle compressible flows with shocks. For parallelization, the Message-Passing Interface library is used; the AMR is handled by the PARAMESH library.

We set up a stratified gas at 1.1×10^4 K initially in hydrostatic equilibrium. The surface mass density of the gas, $\Sigma_{gas} = 7.5 M_{\odot} \text{ pc}^{-2}$. The computation box contains a volume of $(0.5 \text{ kpc})^2 \times (10 \text{ kpc})$, elongated in the vertical direction. At 1.95 pc resolution, it effectively contains $256^2 \times 5120$ zones. We modify the refinement and derefinement criteria so that it becomes gradually more difficult to refine (and easier to derefine) with increasing distance from the midplane ($z = 0$). In practice, the inner ~ 600 pc near the midplane ends up refined to the maximum level. This allows us to capture the vertical flow, while not unnecessarily resolving low-density regions far from the disk. For our fiducial model, the number of dynamically allocated zones is only 7–8 % of that in a single mesh code with the same maximum resolution.

The gravitational potential of Kuijken & Gilmore (1989) is employed. It yields the vertical gravitational acceleration

$$g(z) = -\frac{a_1 z}{\sqrt{z^2 + z_0^2}} - a_2 z, \quad (1)$$

where $a_1 = 1.42 \times 10^{-3} \text{ kpc Myr}^{-2}$, $a_2 = 5.49 \times 10^{-4} \text{ Myr}^{-2}$, and $z_0 = 0.18 \text{ kpc}$. The two terms on the RHS of the equation

represent contributions from a stellar disk and a spherical dark halo. It is static in time; self-gravity of the inhomogeneous, evolving gas is not included. Outflow boundary conditions are used on the upper and lower surfaces parallel to the Galactic plane, while periodic boundary conditions are used elsewhere.

For each supernova explosion, we add thermal energy $E_{sn} = 10^{51}$ ergs in a small sphere whose radius varies as a function of the local density. The radii are chosen such that radiative losses inside the spheres are negligible in the first few timesteps after the explosions. The details are laid out in § 2.3 below. We assume a constant overall rate of supernova explosions, and treat it as an input parameter. This assumption of constant supernova rate is justified by the fact that dynamically important variations in the supernova rate occur on ~ 1 Gyr time scale, far longer than the duration of our simulations.

In addition, each supernova produces ~ 500 metal particles that evolve passively following the gas component. We tag each particle with a unique number and follow its position, velocity, and thermal properties of the gas (density, temperature, and pressure) in the cell that contains the particle. These variables are recorded at every timestep for all particles. This procedure enables us to trace the thermal history of metal particles and to estimate their escape fraction from the galaxy.

We assume that a fixed fraction (15/31 in the fiducial model; § 2.3) of the supernovae are closely correlated in space as a way of simulating superbubbles. The remaining explosions have random positions scattered through the galaxy mass to represent field supernovae.

We solve the standard hydrodynamic equations, namely the continuity equation, the momentum equation, and the energy equation in a background gravitational field. Here we write only the energy equation in our model, which is modified to include supernova heating. In conservative form,

$$\frac{\partial \rho E}{\partial t} + \nabla \cdot [(\rho E + P)v] = \rho v \cdot g - n^2 \mathcal{L} + S, \quad (2)$$

where ρ , P , v , and T denote density, pressure, velocity, and temperature of the gas; the specific total energy E is the sum of internal energy ε and kinetic energy per unit mass: $E \equiv \varepsilon + |v|^2/2$. Gas pressure is related to density via the relation $P = (\gamma - 1)\rho\varepsilon$ with the adiabatic index $\gamma = 5/3$. The gravitational acceleration $g = g(z)\hat{z}$ given by equation (1). The net cooling rate per unit volume $n^2 \mathcal{L} = n^2 \Lambda(T) - n\Gamma(z)$, where n is the number density of gas. For the cooling function, $\Lambda(T)$, radiative cooling appropriate for an optically thin plasma with $Z/Z_\odot = 1$ (cosmic abundance) is included assuming equilibrium ionization (Sutherland & Dopita 1993). It is displayed in Figure 1, approximated as a piecewise power law. When the cooling function is expressed as $\Lambda_i(T) \propto T^{\beta_i}$, the gas is thermally stable where $\beta_i \geq 1$. For the particular cooling curve that we adopted, the gas is thermally stable for $10\text{ K} \leq T < 40\text{ K}$ and $10^4\text{ K} \leq T < 1.7 \times 10^4\text{ K}$, and marginally stable for $40\text{ K} \leq T < 200\text{ K}$. The portion of the curve at low temperatures ($T \leq 2 \times 10^4\text{ K}$) is adopted from Dalgarno & McCray (1972) assuming an ionization fraction of 10^{-2} . The cooling rate is most uncertain in this regime since the approximation of thermal equilibrium is usually invalid. Also shown in dotted line in Figure 1 is the cooling curve from Spaans & Norman (1997), as reproduced in Wada & Norman (2001; see their Figure 1). The exact forms for the two heating terms in our model, the diffuse heating function $\Gamma(z)$ and the impulsive heating from local supernova explosions $S(x, t)$, are given in §§ 2.2 and 2.3, respectively.

In dense regions, the cooling time $t_{cool} \equiv (\gamma - 1)^{-1} kT / n\Lambda$

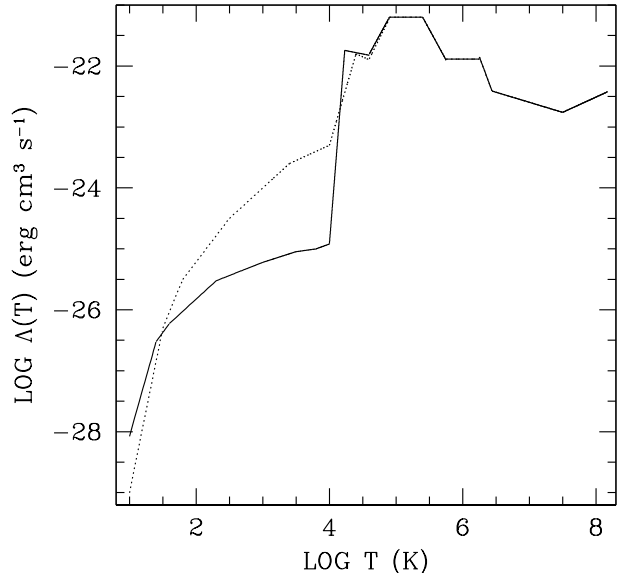


FIG. 1.— Radiative cooling function for an optically thin plasma with $Z/Z_\odot = 1$ approximated as a piecewise power law. The cooling curve is parametrized following Dalgarno & McCray (1972) with an ionization fraction of 10^{-2} at $T \leq 2 \times 10^4\text{ K}$ and Sutherland & Dopita (1993) at $T \geq 2 \times 10^4\text{ K}$. Equilibrium ionization is assumed. For comparison, the cooling curve from Spaans & Norman (1997) is shown in dotted line.

can be shorter than the Courant timestep Δt . FLASH, as a default, applies heating and cooling terms in sequence using an explicit method for updating temperatures. We have combined the separate heating and cooling routines so that temperature is updated only once in each timestep, and used an implicit method whenever the *net* cooling time $t_{net} \equiv (\gamma - 1)^{-1} kT / n\mathcal{L} \leq 0.1\Delta t$. Thus, temperatures for high density ($n \gtrsim 10\text{ cm}^{-3}$) gas are computed using an iterative procedure, in our case, Brent's method (Press et al. 1992).

2.2. Diffuse Heating

It is crucial to choose the right diffuse heating rate. Without this heating, high density gas will simply cool down to T_{min} within a cooling time given by t_{cool} . In other words, no thermal equilibrium will exist above T_{min} . Previous numerical models adopted a diffuse heating rate Γ_{hs} which balances the vertical gravity $g(z)$ on the gas to yield hydrostatic equilibrium at a uniform prescribed temperature T_{init} (Mac Low et al. 1989; Avillez & Breitschwerdt 2004a). This heating rate is computed so that the net cooling rate in equation (2) is zero for all z : $n\Gamma(z) = n^2 \Lambda(T_{init})$, for the hydrostatic equilibrium density profile given in equation 3 below. If the gas were isothermal, the cooling term would dominate where $\rho > \rho_{hs}$, while the diffuse heating term would dominate where $\rho < \rho_{hs}$.

In contrast, photoelectric heating, i.e. photoemission of UV-irradiated dust grains (Bakes & Tielens 1994), has long been thought to be the dominant form of heating for the neutral component of the ISM, i.e., the cold neutral medium (CNM) and the warm neutral medium (WNM) (Wolfire et al. 1995). It has the form $\Gamma_{pe} = 1.0 \times 10^{-24} \epsilon G_0 \text{ erg s}^{-1}$, where the heating efficiency $\epsilon \approx 0.05$ and G_0 is the incident far-ultraviolet field normalized to Habing's (1968) estimate of the local interstellar value (Gerritsen & Icke 1997). We adopt Draine (1978)'s value $G_0 = 1.7$.

Ionizing radiation from OB stars is an additional and a sig-

nificant heating source. Abbott (1982) estimates a total integrated luminosity $\dot{e} = 1.5 \times 10^{-24}$ erg s⁻¹ cm⁻³ in the disk of the Milky Way. Since only 20% of all available UV photons go into heating interstellar gas (Abbott 1982), the photoionization heating rate $\Gamma_{pi} \approx 3.5\Gamma_{pe}$. Much of this heating goes to the warm ionized medium. We do not, however, include it in our diffuse heating rate.

Initially, the gas is assumed to be isothermal. We solve for the hydrostatic equilibrium profile of density for the given gravitational potential (see equation 1):

$$\rho_{hs}(z) = \rho_0 \exp\left(-\frac{a_1\rho_0}{P_0}\left(\sqrt{z^2+z_0^2}-z_0\right)-\frac{a_2\rho_0}{2P_0}z^2\right), \quad (3)$$

where ρ_0 and P_0 are the gas density and pressure at the midplane; $P_0 = (\rho_0/\mu m_H)kT_0$ where T_0 denotes the isothermal temperature of the gas. Note that the profile is narrower than a gaussian by the exponential factor due to a stellar disk (the term containing a_1). This profile, $\rho_{hs}(z)$, would describe the vertical density distribution if the only form of support were thermal pressure. We evolve the systems for sufficiently long periods of time so that the memory of the initial condition is completely lost.

Attempting to balance radiative cooling and diffuse heating of gas at our chosen initial gas temperature $T_{init} = 1.1 \times 10^4$ K leads to $\Gamma_{hs} \approx 30\Gamma_{pe}$. We believe that Γ_{hs} , as used in previous models, is unrealistically high. It is the combination of proper (in fact, much lower) diffuse heating and supernova heating that together should balance radiative cooling.

For the diffuse heating rate in our fiducial model, we adopt Γ_{pe} , a value consistent with Wolfire et al. (1995). Note that our value of Γ is lower than that in Avillez & Breitschwerdt (2004a) by a factor of ~ 18 (their $T_{init} = 9.0 \times 10^3$ K. The heating rate coefficient Γ is assumed to be independent of gas density; according to Wolfire et al. (1995), photoelectric heating weakly depends on density: $\Gamma_{pe} \propto \rho^{0.2}$.

The diffuse heating is applied to gas with $T \leq T_{ion}$, where $T_{ion} = 2 \times 10^4$ K is the temperature at which hydrogen is fully thermally ionized. It is also assumed to decline exponentially in z as $\Gamma \propto \Gamma_0 e^{-z/H_{dh}}$. This exponential factor is a measure for the escaping ionizing radiation from the disk (Domgörgen & Mathis 1994; Dove & Shull 1994; Bland-Hawthorn & Maloney 1999, 2002), which should in principle be treated in a self-consistent way via a radiative transfer code (Fujita et al. 2003; Wood et al. 2004). Existing observations are unable to provide a definite value of H_{dh} for Milky Way type galaxies. In our model, H_{dh} is set to 300 pc so that $\sim 4\%$ of the ionizing radiation leaks out of the disk and into the halo, heating diffuse ionized gas there (Domgörgen & Mathis 1994). At high $|z|$, a minimum value $\Gamma_{min} = 10^{-5}\Gamma_0$ was used. Note that the prescribed functional form for $\Gamma(z)$ precludes the possibility of obtaining thermal equilibrium for the initial gas distribution at all heights.

Our heating function Γ varies as a function of z only and is thus uniform at a given height in the disk (e.g., Gerritsen & Icke 1997). In reality, the diffuse heating rate is extremely non-uniform in space and time; it fluctuates by 1–2 orders of magnitude, and this large fluctuation in the heating rate may be responsible for the conversion of CNM to WNM and vice versa (Parravano et al. 2003; Wolfire et al. 2003). Thus, our use of constant diffuse heating rate is a simplification, justified in part if non-uniformities created by far more energetic supernova explosions dominate the thermal energy budget of the gas.

2.3. Adding Supernova Explosions

One major obstacle that previous large-scale models including supernova feedback have faced was that when thermal energy $E_{sn} = 10^{51}$ erg was added locally into a sphere, most of the energy was radiated away too quickly. This cooling happens within one or two timesteps after the explosion, i.e., before blast waves form and start sweeping up the surrounding medium, converting the initially thermal energy into kinetic energy. As a result, adding impulsive heating in their models did not heat the medium in any significant way either thermally or dynamically (Katz 1992). To avoid this problem, each explosion should occur in such a way that no significant amount of energy is lost radiatively before the expanding sphere forms a strong blast wave and the interior density drops and relaxes to the Sedov profile. In order to achieve this effect, Thacker & Couchman (2001), for example, used an artificial time delay in cooling within the initial explosion sphere. Different algorithms such as assigning the explosion energy to fluid parcels as pure kinetic energy also have problems (Navarro & White 1993). The fundamental cause of this problem is the lack of resolution in these models: relevant length scales for the energy source, in this case supernova explosions, lie below their resolution limits especially in the early phase of the expansion. In many previous models, an ad hoc thermalization efficiency of supernova energy, ranging from 10^{-1} (Navarro & White 1993) to 10^{-4} (Hernquist & Mihos 1995), was assumed. Because we track the thermal and dynamical evolution of blast waves from supernovae explicitly, our model does not suffer from such limitations.

Explosion radii in our model are determined so that the enclosed gas mass within each sphere $M_{exp} = 60M_\odot$ initially. In our fiducial model, this is less than 2×10^{-5} of the total gas mass in the computation box. We neglect the mass ejected by each supernova, i.e., no direct exchange of mass is assumed between stars and the interstellar gas. The radii usually vary between ~ 7 and ~ 50 pc. These initial spheres take up only a small fraction of the total volume. The mean local density inside the sphere is sufficiently low and the timestep is sufficiently short that no delay in cooling is necessary. Inside an explosion sphere, the density is redistributed uniformly to $\rho_{exp} = 3M_{exp}/4\pi r_{exp}^3$, and then a thermal energy E_{sn} is injected evenly into the sphere. The timestep $\Delta t \approx 10^3$ yr. The value of M_{exp} represents a compromise in the sense that too small mass leads to too high cooling rates at $T > 10^8$ K (due to bremsstrahlung) and too few zones within the explosion radius. On the other hand, when the enclosed mass is too large, the initial cooling rates may be again too high if the injected thermal energy heats the sphere only to temperatures $T \lesssim 10^6$ K. Also, the initial explosion sphere may occupy too much volume and thereby introduce artificial changes in the dynamics.

As a preliminary test, we compared the time evolution of thermal and kinetic energies of a single supernova exploding in a uniform background medium (at various densities) with high resolution 1D simulations by Cioffi et al. (1988). At 2 pc resolution, their equation 3.15 provides a good fit for the energy evolution.

The observed supernova frequency for the Galaxy is $1/330$ yr⁻¹ for Type I and $1/44$ yr⁻¹ for Type II supernovae (Tammann et al. 1994). We normalize this to the area of our computation box so that the rates per unit area are 4.0 Myr⁻¹ kpc⁻² and 30.0 Myr⁻¹ kpc⁻². In the vertical direction, the frequency of supernovae is assumed to decline exponentially. The scale

heights for Type I and Type II SNe are 325 pc and 90 pc, respectively (Heiles 1987; Miller & Scalo 1979).

It is known that spatial and temporal clustering of supernovae significantly affects their impact on the ISM (McCray & Snow 1979). However, most numerical simulations so far either completely ignored this correlation or treated clustered supernovae simply as one large constant luminosity wind bubble (Mac Low et al. 1989; Strickland & Stevens 2000). Notable exceptions are Korpi et al. (1999), who used statistical clustering of supernovae by introducing a density threshold for explosion sites, and Avillez (2000) and subsequent work, who assumed that 60% of all supernovae occurred at previous explosion sites. No size distribution of superbubbles was specified by these models. Observations indicate that superbubbles (or stellar clusters) follow a power-law distribution of the form $dN_B \propto n_*^{-2} dn_*$ where n_* is the number of supernovae between a lower cutoff n_{min} and an upper cutoff n_{max} , and dN_B is the number density of superbubbles having a total number of supernovae between n_* and $n_* + dn_*$ (Kennicutt et al. 1988; McKee & Williams 1997; Clarke & Oey 2002). Clarke & Oey (2002) point out that this distribution maximizes the mean volume occupied by each supernova. Interestingly, the n_*^{-2} distribution places equal number of supernovae in any given decade in n_* . This is consistent with the large variations in the number of massive stars in clusters.

For 3/5 of Type II supernovae, we explicitly account for a range of superbubble sizes in terms of the total number of supernovae that they contain, adopting the n_*^{-2} power-law distribution. We fix $n_{min} = 7$. To choose n_{max} , we implement the following simple procedure. According to Kennicutt et al. (1988), there are 6–9 associations with 3500–7000 supernovae in the entire galaxy. Assuming the n_*^{-2} distribution, we choose n_{max} so that there are about A_{gal}/A_{box} associations with $n \in [n_{max}/2, n_{max}]$ supernovae in the Galaxy. If we adopt $A_{gal} = \pi(10 \text{ kpc})^2$ and $A_{box} = (0.5 \text{ kpc})^2$, $n_{max} \approx 40$. In our model, all supernovae that belong to a particular superbubble explode at the same location, an approximation justified by the fact that once a stellar wind bubble forms, all subsequent supernovae explode inside it (Mac Low & McCray 1988). All superbubbles are assumed to have lifetimes of $t_{SB} = 40$ Myr, approximately the age of the least massive B star ($8M_\odot$) when it explodes. We also assume that the given number of supernovae are equally spaced in time over t_{SB} . During the first 5 Myr of each superbubble’s lifetime, we include a constant mechanical luminosity wind originating from 4 pc radius source region, mimicking stellar wind from the O stars. Shull & Saken (1995) argue that such early heating from stellar winds may accelerate shell growth and velocity evolution, compared to constant-luminosity models. The integrated luminosity of stellar wind heating is taken to be $0.14(n_*E_{sn})$ (Ferrière 1995). Mass outflows from stellar winds are not included. Isolated supernovae, which account for the remaining explosions, have random positions scattered throughout the disk. Since the progenitor stars drift apart with velocities $\sim 5 \text{ km s}^{-1}$, they should lie out of their parent clouds by the time they explode, usually $\gtrsim 10$ Myr (for Type IIs) and > 1 Gyr (for Type Ia’s) after they form.

2.4. Missing Physics

Aside from the limited spatial resolution of our simulations, our numerical model neglects several physical processes that are known to participate in interstellar cloud evolution and star formation. For example, since no self-gravity is included in our model, unstable regions do not collapse to form stars;

instead, they just remain dense as a whole, so it is harder for shocks to destroy the clouds. A more complete model in the future should also include magnetic fields as well as shear from galactic rotation. Magnetic fields may substantially thicken swept-up shells (Ferrière et al. 1991) and provide an additional pressure, which may be the dominant component of the gas pressure at low temperatures (Heiles & Troland 2005; Avillez & Breitschwerdt 2004b). A large-scale shear due to differential rotation, when combined with weak magnetic fields, gives rise to the magnetorotational instability, which may dominate the turbulent velocity dispersion in the outer part of the disk (Sellwood & Balbus 1999; Dziourkevitch et al. 2004; Piontek & Ostriker 2005).

Another possibly important yet ignored physical process is thermal conduction. Koyama & Inutsuka (2004) argued for the importance of including thermal conduction by running two models with and without it, which showed discrepant global evolutions of quantities such as kinetic energy and total number of dense clouds. They further argued that, to properly include thermal conduction, the Field length λ_F must be resolved. This is not feasible in our models, where the spatial resolution $\delta x \gg \lambda_F$. However, this crucial role of thermal conduction on cloud formation (via the action of thermal instability) may not carry over to the regime where the medium is externally driven. Based on 2D simulations that included stellar energy injection, Vázquez-Semadeni et al. (2000) suggested that stellar-like forcing erases the signature of the instability, although their models also did not resolve λ_F . Avillez & Mac Low (2002) and Avillez & Breitschwerdt (2004a) also argued that turbulent diffusion may be more important than thermal conduction for mixing gas of different temperatures.

3. RESULTS

3.1. Vertical Direction

For the first few tens of megayears of the simulation, the heating from supernovae is insufficient to counter-balance the gravity. As a result, the disk initially cools and all gas collapses towards the midplane. After the collapse, shock waves bounce back and propagate away from the midplane in both directions, heating the gas at high altitudes. Almost identical behaviors were observed by Avillez (2000). As more supernovae explode, turbulent and thermal pressures build up in the disk. The total kinetic energy in the box exceeds the thermal energy at $t \approx 15$ Myr and thereafter. By $t \approx 30$ Myr, enough supernovae have exploded that the blast waves from the multiple explosions permeate the disk and their interactions regulate the global gas structure. The average gas temperature rises steadily over this period. After $t \approx 60$ Myr, the system reaches a statistical steady state, until the end of our simulation at $t \approx 80$ Myr. The entire run took $\sim 8 \times 10^4$ CPU hours on the TeraScale Computing System at the Pittsburgh Supercomputing Center.

Figure 2(a, b, c) shows typical density, temperature, and pressure variations in the vertical direction, taken at $t = 79.3$ Myr. A clumpy layer of cold dense clouds with a thickness of ~ 200 pc sits in the midplane. Above and below this layer, a galactic fountain (Shapiro & Field 1976) is set up, as observed in the Milky Way, enabling disk-halo interactions. In our model employing the Galactic supernova rate, the time-averaged mean mass flux through any horizontal surface approaches zero, consistent with the negligible fraction of gas escaping the computation box (see below).

The low density gas, which permeates the bulk of the vol-

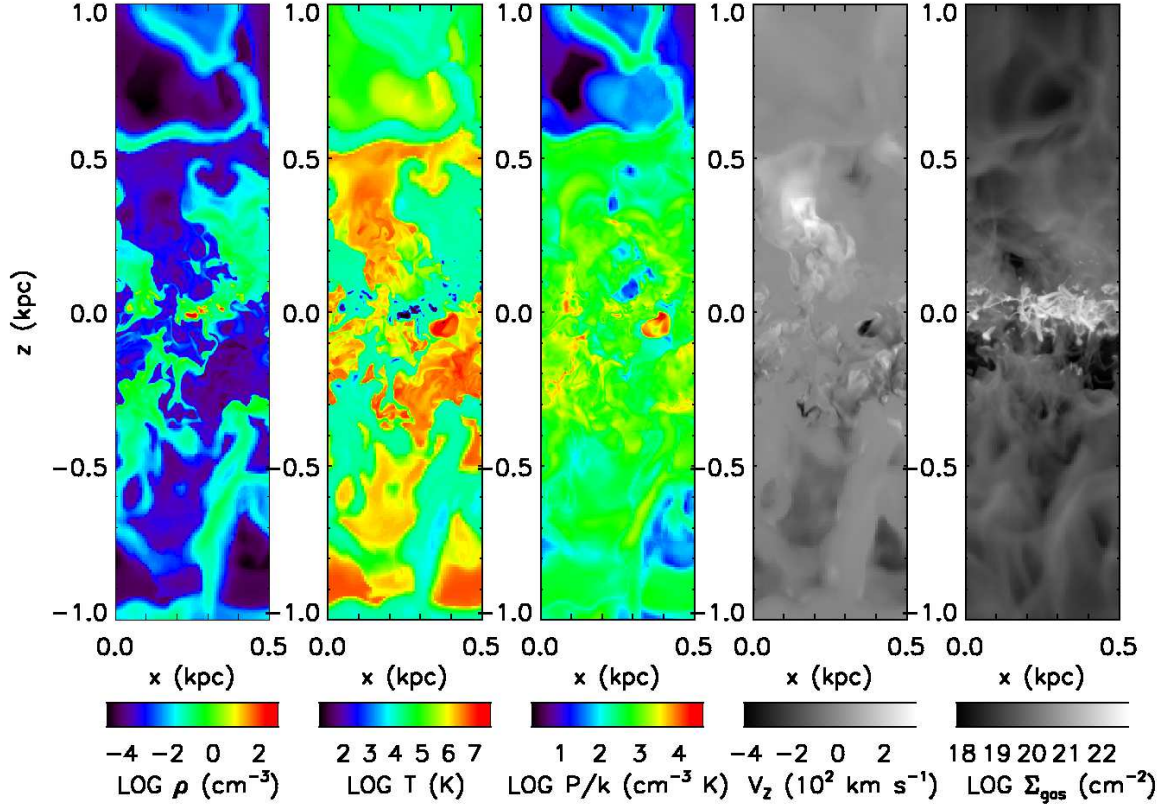


FIG. 2.— Vertical slices of (a) density, (b) temperature, (c) pressure, (d) z component of the velocity, and (e) column density of gas ($\Sigma_y = \int \rho dy$) at $t = 79.3$ Myr. The large shells seen at $z \gtrsim 0.4$ kpc are due to two high-altitude Type I supernovae that exploded 3.9 and 1.5 Myr ago. Note the presence of round cloudlets in (b) and (e) about 100–250 pc away from the Galactic plane. They are fragmented (super)shells and falling towards the midplane at several tens of km s^{-1} . Filaments of neutral gas are found up to ~ 2 kpc away from the midplane. Note that only the inner 2 kpc of our 10 kpc vertical grid is shown.

ume, moves away from the midplane with typical $v_z \approx 10^2$ km s^{-1} . Some expanding superbubbles are launched with z -velocities reaching 300–400 km s^{-1} at the bases. These large bubbles subsequently break out of the disk and directly dispose their thermal energy content to the halo. As the dense gas (predominantly fragments of supershells) rises, its temperature drops because of the decreasing diffuse heating rate as well as radiative cooling of the gas. As a result, neutral gas is present up to ~ 2 kpc above and below the midplane.

Some of that gas later condenses and returns to the disk. This process occurs in several forms. First, cold ($T \approx 10^2$ K in the core) and dense ($n \approx 1 \text{ cm}^{-3}$) cloudlets can be seen 100–250 pc away from the midplane in Figure 2(b, e). These cloudlets fall towards the midplane at velocities of a few to several tens of km s^{-1} . They typically occupy a small volume $\sim (10 \text{ pc})^3$, contain a mass $10\text{--}10^3 M_\odot$, and are structured as a cold dense core plus a lower density tail, embedded in warmer gas. In addition, filaments of neutral clouds are found at larger heights ($|z| \approx 0.25\text{--}2.0$ kpc). With temperatures of order a few thousand degrees, and average densities $\bar{n} \approx 0.3 \text{ cm}^{-3}$, several orders of magnitude higher than their surroundings, these elongated filaments are estimated to contain $10^3\text{--}10^5 M_\odot$ of neutral gas. Some extend beyond several hundred pc in length. Their sizes generally increase with height, but this may be an artificial effect caused by change in spatial resolution. It is tempting to associate the objects within $|z| \lesssim 1$ kpc with intermediate velocity clouds (Wakker 2001). Neutral clouds at even larger heights ($|z| \gtrsim 1$ kpc) may be identified as the tangent point clouds found throughout the inner Galaxy (Lockman 2002). These clouds are thought to contain

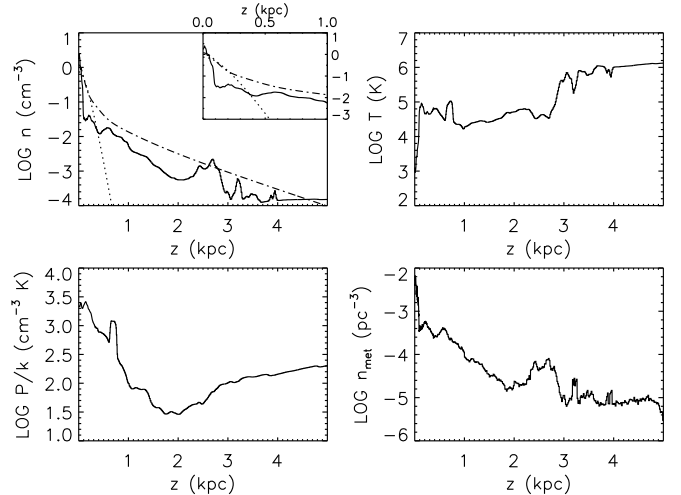


FIG. 3.— Vertical profiles of (a) gas density, (b) temperature, (c) pressure, and (d) metal density at $t = 79.3$ Myr averaged over x - y planes at constant heights. In (a), the dotted line represents our initial isothermal density profile, while the dot-dashed line shows the observed vertical profile of gas, which is the sum of molecular, neutral, and ionized gases. The inset displays an expanded view of the region near the midplane, $|z| \leq 1$ kpc.

a large fraction of the neutral gas in the Galactic halo. Given the crude approximations we make with regard to heating and cooling for the cold dense gas, we consider this a reasonably successful test of the model.

At high altitudes ($z \gtrsim 1$ kpc), extremely hot diffuse gas in the halo has very long cooling times $t_{cool}(n) = 51/n_{-3}$ Myr, where $n_{-3} \equiv n/(10^{-3} \text{ cm}^{-3})$, if we take the cooling rate at

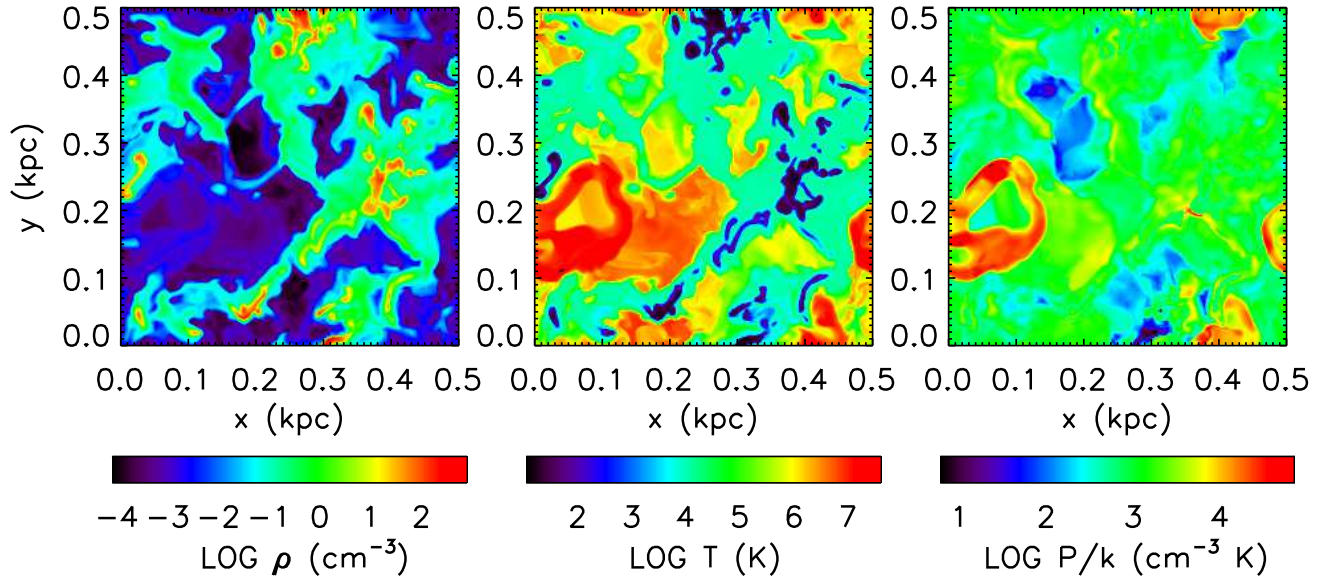


FIG. 4.— Cuts through the midplane ($z=0$) showing distributions of (a) density, (b) temperature, and (c) pressure at $t = 79.3$ Myr. Density and temperature both vary by about seven orders of magnitude. Because of an approximate inverse relationship between the two quantities, thermal pressure changes by 2–3 orders of magnitude. This much variation in pressure is inconsistent with ISM models based on full pressure equilibrium between phases. Correlated supernovae are responsible for producing most of the hot gas in the midplane.

$T = 10^6$ K. Avillez & Breitschwerdt (2004a) ran a similar model for a much longer period (400 Myr) and showed that after $t \approx 70$ Myr the statistical properties related to the vertical distribution of gas do not change appreciably.

Figure 3 shows how the gas density, temperature, pressure, and metal particle density averaged over the x - y plane vary in the vertical direction. For comparison, we show in the dot-dashed line the observed vertical profile of gas, which is the sum of three components: molecular (Clemens et al. 1988), neutral (Dickey & Lockman 1990), and ionized (Reynolds 1991) gases. The average density near the galactic midplane in our model is higher than the observed value by 2–3, while the density is somewhat underpredicted at a few disk scale-heights ($0.1 \text{ kpc} \lesssim |z| \lesssim 0.5 \text{ kpc}$). Uncertainties in observations are large; see, e.g., Figure 10 of Dickey & Lockman (1990). The discrepancy, if real, implies that supernova driving alone cannot quite provide the necessary support in the vertical direction to explain the observed distribution of gas. Additional components of pressure, e.g. from the magnetic field and cosmic rays, are expected to contribute significantly (Boulares & Cox 1990). Compared to our initial isothermal density profile (dotted) in equation 3, a larger amount of gas is present at high altitudes ($|z| \gtrsim 0.5 \text{ kpc}$) due to the presence of a galactic fountain (Fig. 2).

Since outflow boundary conditions are used at the top and bottom surfaces, once the gas escapes with $v_z > 0$, it never returns to the box. For the Galactic supernova rate, only a negligible fraction of the gas ($\sim 0.1\%$) escapes the computation box after 79.3 Myr of evolution. None of the $\sim 3 \times 10^5$ metal particles created during the simulation escapes the grid boundaries at $z = \pm 5 \text{ kpc}$. The vertical distribution of metal particles peaks at the disk midplane, just as that of the gas density does. However, the relative concentration of the metal particles is substantially less pronounced, i.e., an enhancement factor $\sim 10^{3.0}$ instead of $\sim 10^{4.3}$ for the gas density, implying that metals are mostly associated with the warm or the hot gas

phases that have larger scale heights than the cold gas.

For comparison, we ran a model with eight times the Galactic supernova rate and four times the gas column density, scaled so that the Kennicutt relation is approximately satisfied for the computation box. Galactic outflows of mass and metals are observed in this model. We will discuss the vertical structure of the gas in models with higher supernova rates in Paper II.

3.2. In the Midplane

Figure 4 displays distributions of density, temperature, and pressure on a horizontal slice through the midplane ($z=0$) at $t = 79.3$ Myr. As the standard blast wave theory (Ostriker & McKee 1988) predicts, when the age of a supernova remnant approaches the cooling time of the shock-heated gas, the outer part of the bubble undergoes thermal instability and develops a dense spherical shell. These shells collide with one another to form clouds that are filamentary in shape. The clouds have characteristic lengths of several tens to hundred parsecs. Note that these cold dense clouds form even in the absence of self-gravity, as previous numerical simulations have found (Rosen et al. 1993; Rosen & Bregman 1995; Korpi et al. 1999; Avillez 2000). They are formed due to the collective effect of thermal instability and supersonic turbulence. These clouds have temperature lower than 50 K, H_2 formation times of ~ 1 Myr (Hollenbach & McKee 1979), and estimated masses ranging from $\sim 10^3 M_\odot$ to $\sim 5 \times 10^5 M_\odot$. Hence, they can be identified as molecular clouds or giant molecular complexes observed in the ISM. Although in reality many of these clouds contain small scale sub-structures, such details are unresolved in our model. An analysis of the velocity field reveals that turbulent flows within the clouds are trans-sonic or supersonic on the cloud scale (see Fig. 10c; Paper II).

Comparing Figures 4(a) and (b) reveals an approximate inverse relationship between density and temperature. The highest gas density reaches $\sim 10^3 \text{ cm}^{-3}$, and the temperature ranges from 10 K to $\sim 10^7$ K. Both of these quantities vary by

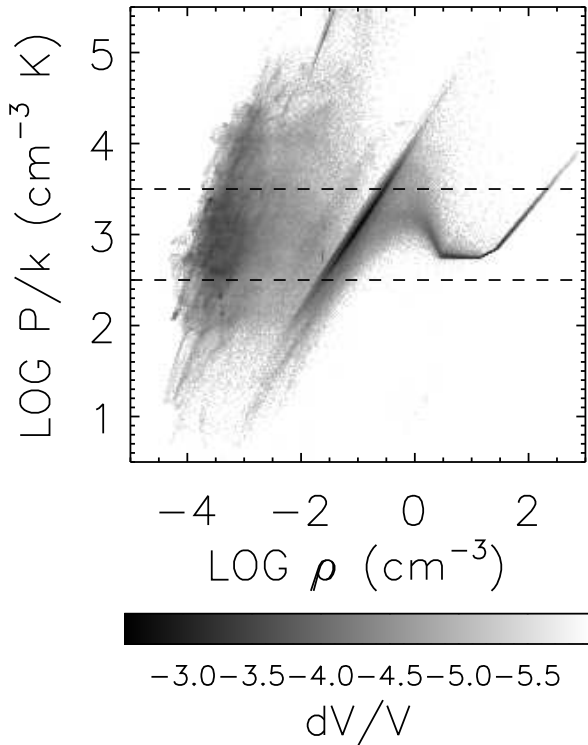


FIG. 5.— Phase diagram showing the distribution of thermal pressure and density in the galactic midplane computed from eight time slices spanning 7.0 Myr of time interval (from 72.3 to 79.3 Myr). The grey scale shows the logarithm of the occupied gas volume. A considerable amount of gas is found in the thermally unstable regime ($200 \leq T \lesssim 1.0 \times 10^4$ K). The straight lines in the upper left quadrant of the diagram are caused by the adiabatic expansion ($P \propto \rho^\gamma$) of young supernova remnants. Hence, the lines have a slope equal to the adiabatic index of gas $\gamma = 5/3$. Interiors of young supernova remnants are associated with low densities and high pressures ($P/k \gtrsim 10^4$ cm $^{-3}$ K). Thermal pressures in dense clouds reach values about an order of magnitude higher than the mean pressure in the general ISM, even in the absence of self-gravity.

more than six orders of magnitude in the midplane. If they had an exactly inverse relationship, the thermal pressure would have been constant. However, as shown in the pressure map (c), there are regions that clearly depart from pressure equilibrium. High pressure regions are usually associated with interiors of newly formed supernovae, shock-compressed regions, or dense cloud cores, whereas low pressure regions are often interiors of old supernova remnants. Overall, thermal pressure varies by 2 to 3 orders of magnitude, confirming the results of previous works (Padoan et al. 1997b; Passot & Vázquez-Semadeni 1998; Mac Low et al. 2005). This much variation in pressure is inconsistent with ISM models based purely on pressure equilibrium between phases induced by thermal instability (Field et al. 1969).

For a detailed look at the pressure distribution, we display in Figure 5 a scatter plot of pressure vs. density (a phase diagram). Two stable branches of the thermal equilibrium curve ($T \approx 10^4$ K and 10 K $\leq T \leq 40$ K) are densely populated. However, other parts of the diagram are occupied by a dynamically determined continuum of densities and temperatures, rather than several discrete phases. This is because lower density gas simply does not have enough time to cool back down to its equilibrium temperature before it gets shock-heated again. If we assume that a supernova shocks, on average, an area $\sim (100 \text{ pc})^2$ in the midplane, for the Galactic supernova rate, the mean time between shock passages will be ~ 1 Myr. This

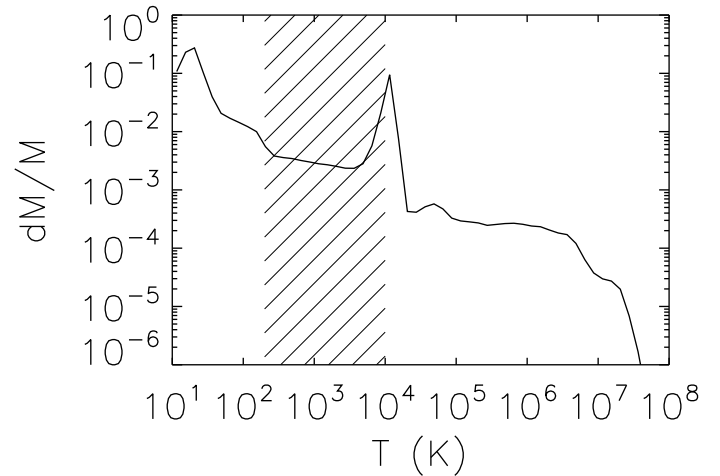


FIG. 6.— Fractions of mass contained in logarithmically spaced temperature bins for gas within 500 pc of the midplane. The hatched region indicates the thermally unstable regime for our cooling curve. Note that the temperature range is more extended than in Heiles (2001), where it ranged from 500 to 5,000 K. Some fraction of the cold gas (X_m) having temperatures below ~ 25 K is expected to be molecular hydrogen.

is much longer than the cooling time, ~ 50 Myr, for the gas having $n = 10^{-3}$ cm $^{-3}$ and $T = 10^6$ K. A new physical description is required for this explosion-dominated medium (Mac Low & Klessen 2004).

Remarkably, $\sim 70\%$ of the points lie in a narrow range of pressure (P/k) between $10^{2.5}$ and $10^{3.5}$ cm $^{-3}$ K. This implies that the low to intermediate density ($n \lesssim 10^2$ cm $^{-3}$) ISM on several hundred pc scales should be described by a nearly isobaric equation of state, instead of an isothermal one, as typically assumed in many recent works on galaxy formation. The near-isobaric character of the medium is reinforced by the distribution of turbulent pressure, as detailed in Paper II.

Physical quantities in our model can be compared directly with existing observations. In particular, we focus on several global quantities measured via H I absorption line studies (Heiles 2001; Heiles & Troland 2003). They found: (1) $>48\%$ of the WNM by mass lies in thermally unstable temperature range; (2) $\sim 60\%$ of all neutral hydrogen (again, by mass) is in the WNM; and (3) The warm gas occupies $\sim 50\%$ of the volume in the Galactic plane.

The distribution of mass in terms of gas temperature is displayed in Figure 6. Based on the shape of our cooling curve, $T = 200$ K separates the CNM from WNM. The WNM ranges from 200 K to 1.7×10^4 K. Some fraction of the cold gas is expected to be molecular hydrogen. According to Heiles (2001), most of the mass in the CNM is contained in gas with temperatures between 25 K and 75 K. It is then reasonable to assume a large fraction of colder gas ($T < 25$ K) to be molecular hydrogen. We denote this mass fraction by X_m , and argue that X_m is close to unity. Adopting these definitions, we find: (1) 67% of the WNM by mass is in the thermally unstable regime; (2) 53% of all H I is contained in the WNM for $X_m=1$ (43% for $X_m=0.9$); and (3) The warm gas occupies 43–52% (49% on average) of the volume in the midplane. Overall, the results are broadly consistent with the observations despite our neglect of magnetic fields and self-gravity.

Typical hot gas filling factors in the midplane of our model $f_h \approx 41$ –51% ($\langle f_h \rangle = 44\%$; see Fig. 4b). These values of

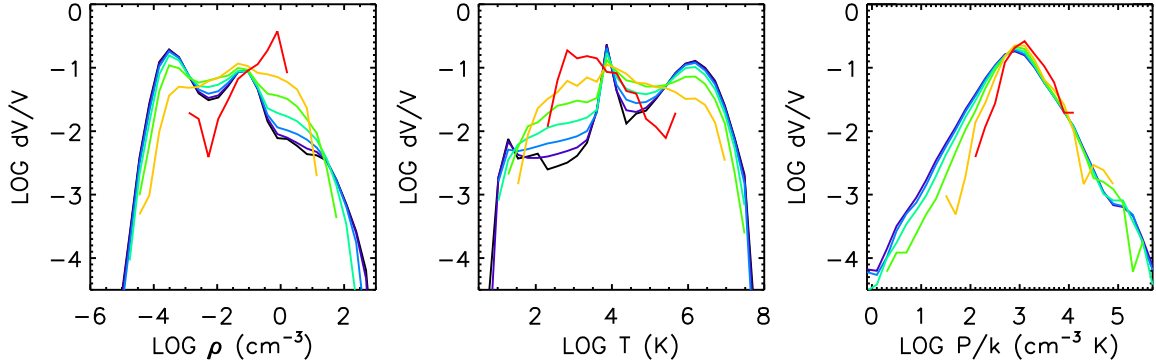


FIG. 7.— Probability density functions for (a) gas density, (b) temperature, and (c) pressure of gas near the midplane ($|z| \leq 125$ pc), taken from eight snapshots spanning 7.0 Myr (from 72.3 to 79.3 Myr). The sizes of subboxes (kernels) used to construct the PDFs increase by factors of 2 from black (1.95 pc) to red (125 pc). The temperature PDF (b) demonstrates the extent to which the classical three-phase medium description is valid. The pressure PDF (c) shows that there is as much volume below the average pressure as there is above it.

f_h are lower than the estimate by McKee & Ostriker (1977) ($f_h \approx 70\%$). They ignored supernova clustering and the vertical density stratification, which are expected to reduce f_h . For example, models that include superbubble evolution predict $f_h \approx 17\text{--}20\%$ near the solar circle (Heiles 1990; Ferrière 1998). The interstellar magnetic pressure will further decrease the volume occupied by hot gas by resisting the expansion of bubbles (McKee 1990; Ferrière et al. 1991; Slavin & Cox 1993). Existing observations of the hot interstellar gas are too limited to constrain f_h , but in external galaxies it is thought that $f_h \lesssim 0.5$ (Detmar 1992; Brinks & Bajaja 1986).

Contrary to our result, Avillez & Breitschwerdt (2004a) obtained low $f_h \approx 0.2$ at 1.25 pc resolution. Their model is discrepant from ours in at least the following three aspects, each of which contributes to lower f_h : (1) Their background heating rate was higher by a factor of ~ 18 ; (2) Their supernova rate was lower by ~ 1.7 ; and (3) They allowed Type II supernovae to explode only in cold ($T \leq 100$ K) and dense ($n \geq 10 \text{ cm}^{-3}$) regions, while we used random locations. Higher background heating rates effectively shift the thermal equilibrium curve (see Fig. 5) diagonally—upward and to the right. As a result, the stable branch of the curve at $T \leq 40$ K mostly lies outside the pressure range occupied by the bulk of the gas. Since the mean thermal pressure in the midplane does not change when Γ is increased, this leads to less gas in the cold phase and more gas in the warm phase. We experimented by running two models with cooling curves determined using ionization fraction of 10^{-1} , as adopted by Avillez & Breitschwerdt (2004a). When we applied 4.5 times the diffuse heating rate of our fiducial model, $f_h \approx 50\text{--}60\%$. We then restarted the model at $t = 68$ Myr, and increased the diffuse heating rate to 18 times the fiducial value. After only 5 Myr of evolution, the volume filling fraction of the hot gas dropped to 35%. Instead, the warm gas occupied 50% of the midplane area. However, we believe that this elevated level of diffuse heating is unphysical. Using density and temperature thresholds for supernova locations lowers f_h because (1) The supernovae then destroy massive clouds, returning the gas to the intercloud medium; and (2) Supernovae that occur in dense regions occupy smaller volumes when integrated over their lifetimes (Clarke & Oey 2002). The results in Korpi et al. (1999) can be interpreted using similar arguments.

3.3. Density Fluctuations

3.3.1. Probability Density Function

There are numerous ways to characterize density distributions of gas. The simplest and the easiest to interpret is the probability density function (PDF) for the gas density. It is displayed in Figure 7(a). We use various subbox sizes over which density PDFs are computed. Purple corresponds to the smallest cubic subboxes with 3.91 pc on a side, and red to the largest subboxes with 125 pc on a side.

We find that most of the simulation volume is occupied by low-density gas due to supernova feedback, in accord with Slyz et al. (2005), who simulated turbulent interstellar medium models in a non-stratified $(1.28 \text{ kpc})^3$ box with periodic boundary conditions and ≥ 10 pc resolution. Stellar feedback and/or self-gravity of gas were included in some of their models. In terms of the density PDF, they found that (1) The models without stellar feedback showed log-normal PDFs with a single peak; (2) A power-law tail developed in the high-density end when self-gravity was included; and (3) The PDF became markedly bimodal when stellar feedback was included, regardless of whether self-gravity was included or not.

Although our PDF is not bimodal, there is a hint of a broad peak near $n = 10 \text{ cm}^{-3}$ for the (thermally stable) cold high-density gas. It is controversial if this part of the PDF can be approximated by a log-normal function. Using 2D simulations including heating, cooling, and self-gravity, Wada & Norman (2001) claim the high-density end of their density PDFs is well-fitted by a log-normal function (see their Figure 16). In contrast, several numerical experiments that included either self-gravity of gas or non-isothermal equation of state ($\gamma \neq 1$) reported that high-density tails develop in non-isothermal cases (Scalo et al. 1998; Li et al. 2003). Although a log-normal density PDF is a natural outcome for isothermal gas (Passot & Vázquez-Semadeni 1998), support for such a PDF for non-isothermal cases remains weak.

The one-point density PDF does not contain information on how dense regions or voids are connected in space. For this reason, the cloud mass spectrum cannot be derived from the density PDF alone, as Scalo et al. (1998) point out. To supplement the density PDF, we attempt two methods of analysis. First, Figure 7(a) shows how the density PDF changes as the subbox size increases. That the PDFs show markedly different shapes attests to the importance of specifying the smooth-

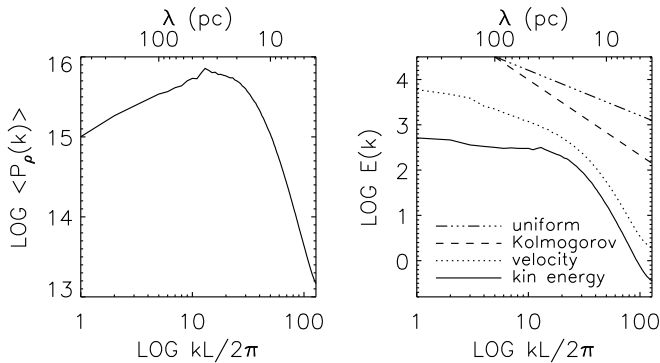


FIG. 8.— (a) Angle-averaged density power spectrum, displaying a wide peak around $kL/2\pi \approx 20$. The box size $L = 0.5$ kpc. The power falls off at large wavenumbers (small wavelengths) due to numerical diffusion. (b) Kinetic energy spectrum (solid) and angle-averaged velocity power spectrum (dotted). The kinetic energy is distributed over a wide range of wavenumbers. There is no single effective driving scale, unlike in Kolmogorov’s idealized picture of incompressible turbulence. We find that 90% of the total kinetic energy is contained in wavelengths $\lambda \leq 190$ pc. Because of the highly intermittent density structure, the velocity power spectrum is not parallel to the kinetic energy spectrum, especially at large scales. To guide the eye, two straight lines are plotted: the Kolmogorov energy spectrum (dashed) and the spectrum containing an equal amount of energy per decade (dot-dashed).

ing scale with which the density PDF is measured. More significantly, the Jeans mass M_J and the density threshold for gravitational collapse ρ_{th} also change as a function of scale (see Fig. 10). Despite the fact that we do not fully understand what determines the shapes of the PDFs as the subbox size increases, this clearly has implications for gravitational collapse, as we explore in § 4.

3.3.2. Power Spectrum

The other method to characterize density fluctuations is to use second-order statistics such as the auto-correlation function or its Fourier transform (FT), the power spectrum. Our computation box is periodic in the x and y directions but non-periodic in z , while FFTs assume periodicity in all directions. Hence, before taking FFTs, we apply to the z -components of the variables the Hanning window defined by $w(z) = (1/2)(1 + \cos(2\pi z/L_z))$ where L_z is the vertical extent of the box used for the FFT (0.5 kpc) and $-L_z/2 \leq z < L_z/2$.

While the velocity power spectrum in an incompressible medium $|v(x)|^2$ has the clear physical meaning of specific kinetic energy (see the discussion of Parseval’s theorem in § 3.4), $\rho(x)^2$ does not. If the density PDF turns out to be log-normal and if $s \equiv \log \rho$ can be taken as a Gaussian random variable, a power spectrum of s can completely specify the density distribution. Even though this is not the case (see Fig. 7a), the density power spectrum is nevertheless useful for comparison with previous numerical models.

The density power spectrum of an explosion-driven, strongly compressible medium is displayed in Figure 8(a). Its shape contrasts drastically with its counterpart in a weakly compressible medium, where density fluctuations behave as a tracer field and possess a Kolmogorov spectrum (Lithwick & Goldreich 2001). The spectrum peaks near the smallest scale at which kinetic motions can be well-resolved $\lambda_\rho \approx 20$ pc. This wavelength is slightly smaller than the most energy-containing scales $\lambda_E \approx 20\text{--}40$ pc (Fig. 8b). Since λ_ρ is within the range affected by numerical diffusion (§ 3.4), this conclusion is somewhat uncertain. We do note that our value of λ_ρ is comparable to the correlation length of 28 pc measured from two-dimensional autocorrelation functions of the molecular

hydrogen column density map in the Taurus molecular complex (Kleiner & Dickman 1984).

It is simple to predict the density power spectrum of a medium dominated by shocks, because a shock is essentially a step function in density and velocity fields. Step functions are generally associated with power spectra having $P(k) \propto k^{-2}$ (Passot et al. 1988). However, neither observations nor numerical simulations support this relation for density. Padoan et al. (1997a) showed that the density power spectrum has a power-law form $P(k) \propto k^{-\alpha}$ with $\alpha = 2.6 \pm 0.5$, similar to values determined from observations (Stutzki et al. 1998). However, comparison with observations is not straightforward, since only the projected (column) density, not the physical density, is available from observations. The steep spectral slope at larger wavenumbers may have been caused by the nature of PPM; see § 3.4. Unlike the spectrum in Padoan et al. (1997a) who used a periodic isothermal box, our density spectrum turns over at $kL/2\pi \approx 10$ and falls off at small wavenumbers (large wavelengths).

Finally, we add a cautionary note. Generally, one should be careful when computing power spectra of physical quantities from an AMR code. This is because power at small scales can be easily underestimated in relatively under-refined regions. To avoid such mistake, the choice of refinement and derefinement criteria is crucial (Kritsuk et al. 2004). Although our simulations are performed with an AMR code, the region near the midplane, particularly the cube with volume $(500 \text{ pc})^3$ within $|z| \leq 250$ pc, ends up refined uniformly to the maximum refinement level after a few tens of Myr of evolution due to extreme density inhomogeneities and turbulent motions caused by the explosions. (For this reason, in fact, we effectively turn off the AMR machinery at late times.) Thus, at late times, we may compute power spectra without misrepresenting them.

3.4. Energy Fluctuations: Driving Scale

How is the kinetic energy distributed among various length scales in our turbulent medium stirred by supernova explosions? This question is crucial for star formation. Depending on the slope of the forcing function $k^{-\alpha}$, the statistics of turbulent fluctuations and clumps change (Bonazzola et al. 1987; Biferale et al. 2004).

Previous simulations of uniformly driven (as opposed to explosion-driven) turbulence with variable driving wavelengths have shown that the occurrence and efficiency of local collapse into dense cores—and, presumably, stars—decreases as the driving wavelength decreases (KHM00). Despite its relevance to cloud formation, as far as we know, the driving scale has never been measured in numerical simulations of ISM driven by point explosions. Observations of molecular clouds show that power-law scaling extends up to the largest observed clouds (Ossenkopf & Mac Low 2002), and suggest that the turbulence is driven by large-scale, external sources. However, gas density and velocity—two physical quantities relevant to the kinetic energy density—can only be disentangled by observations under certain conditions (Brunt & Mac Low 2004; Lazarian & Esquivel 2003).

In an incompressible or weakly compressible medium, gas density is nearly uniform and thus the energy spectrum is simply the angle average of the velocity power spectrum: $E_{inc}(k) = 4\pi k^2 \langle P_v(k) \rangle_\Omega$ where $k = |k|$ and $P_v(k)$ is the three-dimensional Fourier transform of each component of v , squared and then summed. The velocity power spectra of compressible interstellar gas have been studied in 2D

(Dahlburg et al. 1990; Vázquez-Semadeni et al. 1996; Wada & Norman 2001) and in 3D (e.g., Kritsuk et al. 2004). However, none of the previous simulations performed in 3D dealt explicitly with power spectra of the medium driven by discrete physical space forcing.

In a strongly compressible medium with high Mach numbers, the gas density ρ is highly intermittent and can vary by several orders of magnitude. To measure how much kinetic energy is contained near a given wavenumber k , we should compute the power spectrum of $\sqrt{\rho}v$ instead of v , since according to Parseval's theorem:

$$\int_{-L/2}^{L/2} [f(x)]^2 dx = \int_0^\infty [|\hat{f}(k)|]^2 dk, \quad (4)$$

where $f(x)$ and $\hat{f}(k)$ are Fourier transform pairs, and L is the size of the periodic box. If we substitute $v_i(x)$ for $f(x)$ (where $i = x, y, z$), we obtain a relation for the incompressible case, which justifies the use of the velocity power spectrum for the kinetic energy spectrum. If we now substitute $\sqrt{\rho}v_i$ in place of $f(x)$, we obtain the corresponding relation for a compressible medium, which relates the kinetic energy density (ρv_i^2) to the Fourier transform of $\sqrt{\rho}v_i$. As we demonstrate below, the power spectrum of $\sqrt{\rho}v$ shows a markedly different shape from that of v . This point was briefly noted in the discussion of Padoan & Nordlund (1999).

Figure 8(b) shows the one-dimensional kinetic energy spectrum $E_{kin}(k) = 4\pi k^2 \langle P_w(k) \rangle_\Omega$ where $w \equiv \sqrt{\rho}v$. The measured slope is far shallower than the Kolmogorov spectral index of $-5/3$ for incompressible turbulence. In a strongly compressible, explosion-driven turbulence, shocks and interacting blast waves contribute to a wide range of driving wavelengths. The shallow spectral slope shows the presence of substantial power at small length scales, suggesting that SN-driven motions dominate the kinetic energy spectrum even at small scales where H II regions (Haverkorn et al. 2004) or protostellar outflows may also be active. Thus, turbulence in the dense medium is at least partly driven by supernovae.

The angle-averaged velocity power spectrum often used in the literature is also plotted in Figure 8(b) for comparison. This spectrum contains velocity information only and neglects the density inhomogeneity, as though the medium were incompressible. The remarkable difference at low wavenumbers between the two spectra in Figure 8(b) suggests that dense regions, which more or less determine the shape of the kinetic energy spectrum, have a vastly different velocity structure from rarefied (intercloud) regions.

Although kinetic energy is distributed over a broad range of scales, 90% of the total kinetic energy is contained on wavelengths $\lambda \leq 190$ pc. This value (190 pc) is likely to decrease somewhat in higher resolution simulations that better resolve turbulent motions on $\lesssim 20$ pc scales. In typical cosmological simulations, therefore, most of the turbulent energy due to multiple supernova explosions is contained in scales smaller than a resolution element. To include the effect of hydrodynamic feedback in such simulations, it is necessary to use a subgrid model that represents unresolved, small-scale motions (Paper II).

To test the robustness of our results on numerical resolution, we ran our fiducial model with the same box size at three different resolutions (8, 4, and 2 pc). The energy power spectra for the three runs display identical shapes in the dissipation range, but are shifted horizontally with respect to one another by ~ 2 . This occurs because, in a compressible medium, structures on scales smaller than ~ 10 grid zones are affected by

numerical dissipation (Porter et al. 1992; Mac Low & Osenkoff 2000), determining the inertial range of the turbulent cascade. Finite difference algorithms directly damp kinetic motions on small scales and convert their kinetic energy into heat. It follows that velocity differences on small scales ($\lesssim 10\Delta x$) are somewhat underestimated. However, that may not affect the overall dynamics since thermal pressure should dominate the turbulent pressure on such small scales.

The power spectra tend to flatten slightly near the wavenumber of maximum dissipation. This distinctive shape of the spectrum in the dissipation range ($\lesssim 10\Delta x$) is caused by the bottleneck effect known to occur in hydro codes using PPM (Falkovich 1994; Porter et al. 1992; Porter et al. 1998).

3.5. Velocity Structure Function

The velocity power spectrum is steeper than the slope expected for Kolmogorov turbulence ($-5/3$). In addition, since the spectral slope varies depending on the wavenumber, it is unclear whether an inertial range exists at all. How can we understand this behavior? Extensive experimental and numerical studies have found deviations from the Kolmogorov spectrum, usually referred to as intermittency corrections. To quantify deviations from the Kolmogorov spectrum, it is useful to compute a velocity structure function defined by

$$S_p(l) = \langle |v(x+l) - v(x)|^p \rangle \propto l^{\zeta(p)}, \quad (5)$$

where the scalar lag $l = |l|$. There are several phenomenological frameworks for compressible turbulence, each of which gives a distinct prediction for the scaling exponents $\zeta(p)$. We apply the idea of extended self-similarity, which showed correct scaling behaviors for $\zeta(p)$ even in systems with moderate Reynolds numbers, specifically the power index $-(1 + \zeta(2)) = -1.74$ for a relatively wide range in $S_3(l)$ (Benzi et al. 1993; Camussi & Benzi 1996). We plot the structure function against the third-order structure function $S_3(l)$ in Figure 9(a).

Predictions for $\zeta(p)$ from various analytic theories of turbulence are shown in Figure 9(b). Based on She & Leveque (1994)'s model of intermittency for incompressible turbulence (see also She & Waymire 1995), Boldyrev (2002) proposed an extension, noting that the most dissipative structures in strongly compressible ISM tend to be shocks, i.e. two-dimensional sheets. Our structure functions for the transverse component of the velocity field are most consistent with the prediction from this theory. Those for the longitudinal component diverge from straight lines at large $S_3(l)$ (i.e., large separations), because most of the gas in terms of volume travels away from the midplane. If we omit the last two data points for each value of p , we find that the longitudinal structure functions also agree with Boldyrev (2002)'s prediction. Until our work, the theory has been compared well only with isothermal gas driven on large scales by a random Fourier space forcing (Boldyrev et al. 2002; Padoan et al. 2003). Our result demonstrates that the theory is applicable even to a medium driven by discrete point explosions and subject to nonlinear heating and cooling processes.

4. GRAVITATIONALLY UNSTABLE CLOUDS

The connection between small-scale star formation in local regions of cold dense gas and large-scale, galactic star formation is unclear. The Kennicutt-Schmidt law is successful in predicting star-forming rates (SFRs) of galaxies with wildly different characteristics—from low-surface brightness galaxies to starbursts—implying that the SFR can be estimated

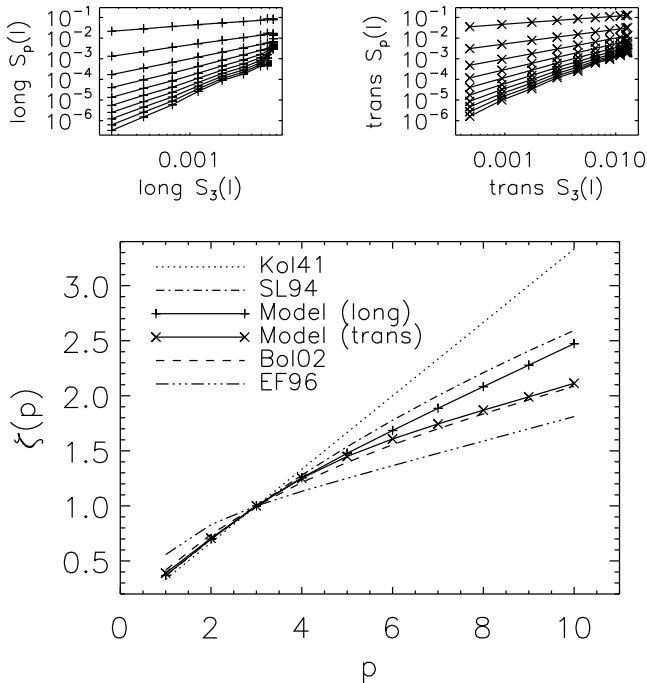


FIG. 9.— (a) Longitudinal and transverse velocity structure functions. (b) Scaling exponents $\zeta(p)$. Theoretically expected scalings are shown for comparison. From top to bottom, they are from Kolmogorov (1941) (dotted), She & Leque (1994) (dot-dashed), and Boldyrev (2002) (dashed). The dot-dashed line is plotted assuming $D = 2.3$, taken from Elmegreen & Falgarone (1996)’s observation of molecular clouds. The data points are from, again from top to bottom: longitudinal and transverse velocity structure functions.

from macroscopic properties of galaxies, and is perhaps controlled mainly by gravitational instability. Such a claim was made by Li et al. (2005), who used an isothermal equation of state for gas with a high speed of sound to represent the interstellar turbulent pressure. One might argue, though, that star formation is inherently a local phenomenon that depends sensitively on the physical conditions on cloud scales.

On kiloparsec scales, much larger than the driving scales of the interstellar turbulence that we measured in § 3.4, gravity is important and the effect of turbulence can be represented as an effective turbulent pressure term (Elmegreen & Scalo 2004). Below those scales, at the scales resolved by our numerical model, supersonic turbulence controls much of the cloudy structure.

Observational and numerical studies have established that the Toomre (1964) parameter $Q \equiv \kappa\sigma/\pi G\Sigma_{\text{gas}}$, where κ is the epicyclic frequency and σ is the effective sound speed, controls whether or not a given region of a galaxy will actively form stars (Klessen 1998; Li et al. 2005). However, even in Toomre-unstable regions, not all the gas collapses within the local freefall time. Several authors have argued that only a fixed (constant) fraction of mass f_M above some density threshold will collapse to form stars (Elmegreen 2002; Krumholz & McKee 2005), based on the universality of density PDFs in turbulent media (Wada & Norman 2001). Still, many questions remain unanswered: what determines f_M ; is there a clear density threshold for star formation; and is f_M the same (on average) for various galaxy types?

One of the aims of our work has been to study how gas dynamics and thermodynamics shape the ISM. In our model, cold dense clouds form directly in the turbulent flow. What fraction of these clouds are gravitationally unstable, given the

density and velocity structures in our model? If gravity is decoupled from other cloud-forming processes such as turbulence and thermal instability, do we still reproduce a star-formation rate consistent with the value implicitly set by the input supernova rate? To answer these questions, we apply to the data a simple criterion for gravitational collapse (see below). By comparing the collapse rate with our input supernova rate, we can quantitatively check the validity of our high-resolution simulations as a model for star formation.

Since our model does not include self-gravity of gas, we estimate the gravitational collapse rate (hence the SFR) by using a crude method that involves the modified Jeans criterion (Chandrasekhar 1951). This approach will yield the correct result only if (1) the spatial resolution of our model is sufficiently high that the gas dynamics is well resolved, particularly physical quantities such as mass density ρ and velocity dispersion of gas σ that are crucial for estimating the collapse rate, and (2) supersonic random motions determine most properties of star-forming molecular clouds, with just minor modifications from gravity (Padoan et al. 1997a; Padoan et al. 1997b; Padoan et al. 1998). If self-gravity extensively alters the structure of clouds presented in § 3, our estimate of the collapse rate will be inaccurate.

We analyze the gas in the rectangular region near the mid-plane within $|z| \leq 125$ pc that contains the bulk (>90%) of the total gas mass. We estimate the total collapse rate of gas as follows. First, we identify Jeans-unstable boxes at varying scales using the criterion $M_{\text{box}}/M_J > 1$, where $M_J = \bar{\rho}\lambda_J^3$, $\bar{\rho}$ is the average density in the box, $\lambda_J = (\pi/G\bar{\rho})^{1/2}\sigma_{\text{tot}}$, and $\sigma_{\text{tot}} \equiv (\bar{c}_s^2 + \frac{1}{3}\bar{\sigma}^2)^{1/2}$ (Chandrasekhar 1951). We use $\bar{c}_s^2 \equiv (1/M_{\text{box}})\int_{\text{box}}\bar{c}_s^2 dM$ and $\bar{\sigma}^2 \equiv (1/M_{\text{box}})\int_{\text{box}}\sigma^2 dM$. (Paper II contains more details on how \bar{c}_s and $\bar{\sigma}$ are computed.) The total velocity dispersion σ_{tot} changes with scale, because kinetic energy is distributed over a wide range of scales (§ 3.4). Then the total collapse rate is estimated assuming that the unstable boxes collapse within the local freefall time. To convert this value to the SFR, we multiply it by a star formation efficiency of 0.30, as it is thought that $\sim 30\%$ of the cloud mass that gravitationally collapses is converted to stars (Li et al. 2005 and references therein).

Figure 10(a) shows that there is no single density threshold ρ_{th} for gravitational collapse. Instead, ρ_{th} depends on the scale at which collapse occurs. The turbulent velocity dispersions for gas with number density of 10^2 cm $^{-3}$ range from 0.1 to 1.0 km s $^{-1}$ (Fig. 10b). For the small (purple and blue) subboxes, the turbulent velocity dispersion is lower than the local sound speed (Fig. 10c), as turbulent motions on those scales are not well resolved in our model.

The plot of the predicted SFR against the subbox sizes is displayed in Figure 11. Our results show that, for $L_{\text{box}} \gtrsim 20$ pc where turbulent motions are resolved, even if all the gas in turbulent Jeans unstable boxes collapses and forms stars within the local freefall time t_{ff} , the resulting star formation rate remains lower than the value consistent with our input supernova rate: 4.4 (or 6.8) $\times 10^{-3}$ M $_{\odot}$ yr $^{-1}$ kpc $^{-2}$, which is computed assuming 130 (or 200) M $_{\odot}$ of stellar mass is required per supernova using the Salpeter IMF.

Turbulent compression and the structuring of the ISM by supernovae may set the stage for further gravitational collapse and even determine where it occurs. However, the discrepancy between the assumed and the predicted SFRs illustrates a limitation of our model. We interpret this as an indication that the density PDF must be affected by self-gravity; this idea

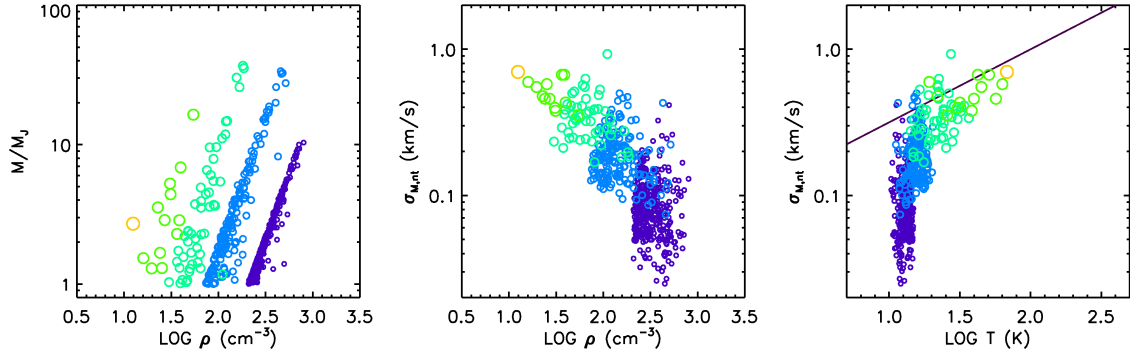


FIG. 10.— (a) Mass contained in each subbox vs. average gas density of the subbox. There is no single density threshold for gravitational collapse. (b) Turbulent velocity dispersion vs. average density of gas in the subbox. (c) Same as (b), but plotted against the mass-weighted gas temperature. Most Jeans-unstable boxes on the cloud scale are associated with transonic or supersonic velocity dispersions.

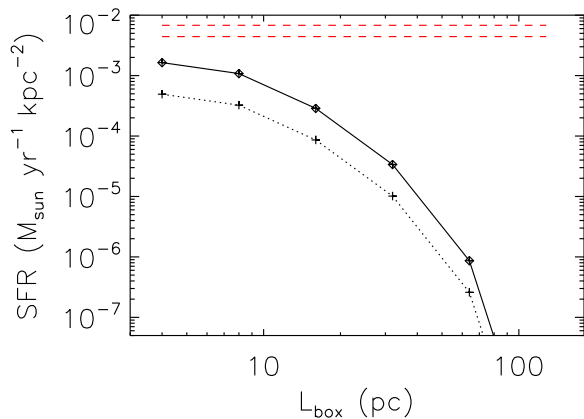


FIG. 11.— Predicted star formation rate from the model plotted against the subbox sizes used. The dotted line is drawn assuming that 30% of the mass in Jeans unstable regions turns into stars. The red dashed lines show the SFRs consistent with the assumed Galactic supernova rate, assuming 130 or 200 M_{\odot} of stellar mass is required per supernova.

is supported by numerical results that the high-density end of the PDF, most crucial for gravitational collapse, is positively skewed when self-gravity is turned on (Li et al. 2003; Slyz et al. 2005). If this is true, computations of SFRs based directly on the assumption of a log-normal density PDF may be misleading. Uncertainties in the present analysis are missing kinetic energy caused by the finite resolution (§ 3.4), which tends to increase predicted SFRs on small scales, and the absence of magnetic fields. Magnetic pressure reduces the probability of collapse (HMK01; Vázquez-Semadeni et al. 2005).

We conclude that, while it may be possible to predict where gravitationally bound regions will occur, estimating the SFR based on our model leads to an underestimate, about an order of magnitude lower than the value consistent with the assumed supernova rate. This limitation of our ISM model probably stems from the key physical process that we ignore: self-gravity of the gas. Other models relying entirely on turbulent compression will likely show similar deficits.

We verified that the gas sitting at a uniform temperature ($T = 4.2 \times 10^3$ K, corresponding to the total (thermal plus turbulent) velocity dispersion of our medium $\sigma \approx 6.5$ km s^{-1}) in hydrostatic equilibrium with the imposed gravitational field is stable. In other words, no Jeans unstable boxes occur. However, this point cannot be used to argue that supernovae en-

hance the global gravitational collapse rate and trigger star formation. In fact, the opposite is true. Since the gas was initially out of thermal equilibrium, it would have promptly collapsed and cooled into a thin sheet. Most of the mass would have become gravitationally unstable, without extra stirring from supernovae. The net effect of supernova-driven turbulence is to *inhibit* star formation globally by *decreasing* the amount of mass unstable to gravitational collapse.

5. SUMMARY

In this work, we have constructed 3D models of the ISM including vertical stratification and discrete physical space forcing by supernova explosions. We included parametrized heating and cooling as well as both isolated and correlated supernovae. This work supports models that treat supernova-driven turbulence as a major structuring agent in the ISM. Our main results are as follows:

- Cold dense clouds naturally form as blast waves sweep the gas and collide. The intercloud region is filled with warm or hot gas having relatively low densities. The resulting density and velocity structures adequately match the observed filamentary and clumpy structure of the ISM.
- A galactic fountain reaching a height of several kiloparsecs forms, with most of the volume moving away from the midplane. Fragmented shells rain back down as small cold clumps, which may be identified as intermediate velocity clouds.
- Global quantities in our model are broadly consistent with existing observations. Specifically, our results are consistent with observations of the mass fraction of thermally unstable gas and the warm gas filling factor in the Galactic plane derived from H I absorption lines (Heiles 2001; Heiles & Troland 2003).
- The diffuse heating rate Γ influences the global structure of our model. For example, in our numerical experiments, increasing Γ by 4 lowered the occupation fraction of the hot gas in the Galactic plane by $\sim 20\%$. This occurs because high background heating rates effectively shift the thermal equilibrium curve in the phase diagram so that the cold (thermally stable) branch lies mostly outside the range of pressure occupied by the bulk of the gas.

- The vertical distribution of gas in our model deviates from the profile inferred from observations. Specifically, the gas is excessively concentrated in the disk midplane by factors of 2–3, while it is deficient at $0.1 \lesssim |z| \lesssim 0.5$ kpc. We attribute this discrepancy to neglected components of pressure such as those from the magnetic field and cosmic rays.
- The density power spectrum has a broad peak close to the dissipation scale $\lambda \sim 20$ pc. It turns over and falls off at large scales.
- There is no single effective driving scale; instead, we see energy injection over a range of scales. As a result, the kinetic energy power spectrum possesses a slope much flatter than Kolmogorov's spectrum at scales between ~ 20 and ~ 500 pc. The predominance of small scale density structure causes the kinetic energy power spectrum to look remarkably different from the often-used velocity power spectrum. About 90% of the total kinetic energy is contained in wavelengths shortward of 190 pc.
- The velocity structure functions demonstrate that the phenomenological theory proposed by Boldyrev (2002) is applicable even to a medium driven by discrete point explosions and subject to nonlinear heating and cooling processes.
- Even if all the gas in turbulent Jeans unstable subboxes in our simulation collapses and forms stars in local freefall times, the resulting collapse rate is significantly lower than the value consistent with the input supernova rate. Supernova-driven turbulence inhibits, but does not prevent, star formation. From this, we infer

that the density PDF must be significantly affected by self-gravity. For predicting physical properties of star-forming regions (such as the stellar initial mass function), the statistics of turbulent fluctuations generated by models without self-gravity can be misleading.

Applying high supernova rates to our model galaxy naturally leads to galactic outflows that have already been observed at both low (Heckman et al. 2000) and high redshifts (Pettini et al. 2001, 2002; Shapley et al. 2003). In the future, we will use these local models to measure the efficiency of energy transfer into superwinds out of a stratified disk for a given star formation rate, and thereby construct subgrid models for stellar energy feedback in cosmological simulations.

We are grateful to M. Avillez, S. Glover, I. Goldman, C. Heiles, L. Hernquist, E. Jenkins, R. Klessen, Y. Li, C. McKee, J. Stone, and S. White for stimulating discussions. We acknowledge a helpful suggestion from G. Bryan regarding the importance of the thermal equilibrium curve in interpreting the relationship between the hot gas filling factor and background heating rate. We thank J. Oishi for valuable comments on the manuscript that improved the presentation and J. Maron for suggesting the use of structure functions. M. K. R. J. was supported by an AMNH Graduate Student Research Fellowship. M.-M. M. L. acknowledges support by NSF Career grant AST99-85392, and NSF grants AST03-07793, and AST03-07854. The software used in this work was in part developed by the DOE-supported ASCI/Alliance Center for Astrophysical Thermonuclear Flashes at the University of Chicago. Computations were performed at the Pittsburgh Supercomputing Center supported by the NSF.

REFERENCES

- Abbott, D. C. 1982, *ApJ*, 263, 723
 Armstrong, J. W., Rickett, B. J., & Spangler, S. R. 1995, *ApJ*, 443, 209
 Avila-Reese, V., & Vázquez-Semadeni, E. 2001, *ApJ*, 553, 645
 Avillez, M. A. 2000, *MNRAS*, 315, 479
 Avillez, M. A., & Berry, D. L. 2001, *MNRAS*, 328, 708
 Avillez, M. A., & Mac Low, M.-M. 2002, *ApJ*, 581, 1047
 Avillez, M. A., & Breitschwerdt, D. 2004a, *A&A*, 425, 899
 Avillez, M. A., & Breitschwerdt, D. 2004b, *Ap&SS*, 292, 207
 Bakes, E. L. O., & Tielens, A. G. G. M. 1994, *ApJ*, 427, 822
 Ballesteros-Paredes, J., Hartmann, L., & Vázquez-Semadeni, E. 1999, *ApJ*, 527, 285
 Benzi, R., Ciliberto, S., Tripicciono, R., Baudet, C., Massaioli, F., & Succi, S. 1993, *Phys. Rev. E*, 48, 29
 Biferale, L., Lanotte, A. S., & Toschi, F. 2004, *Phys. Rev. Lett.* 92, 194503
 Bland-Hawthorn, J., Maloney, P. R. 1999, *ApJ*, 510, L33
 Bland-Hawthorn, J., Maloney, P. R. 2002, *ASP Conf.*, 240, 267
 Boldyrev, S. 2002, *ApJ*, 569, 841
 Boldyrev, S., Nordlund, Å., Padoan, P. 2002, *ApJ*, 573, 678
 Bonazzola, S., Falgarone, E., Heyvaerts, J., Perault, M., & Puget, J. L. 1987, *A&A*, 172, 293
 Boulares, A., & Cox, D. P. 1990, *ApJ*, 365, 544
 Brunt, C. M., & Mac Low, M.-M. 2004, 604, 196
 Brinks, E., & Bajaja, E. 1986, *A&A*, 169, 14
 Camussi, R., & Benzi, R. 1996, *Phys. Fluids Letters*, 9, 257
 Chandrasekhar, S. 1951, *Proc. Royal Soc. London A*, 210, 26
 Cioffi, D. F., McKee, C. F., & Bertschinger, E. 1988, *ApJ*, 334, 252
 Clarke, C., & Oey, M. S. 2002, *MNRAS*, 337, 1299
 Clemens, D. P., Sanders, D. B., & Scoville, N. Z. 1988, *ApJ*, 327, 139
 Cole, S., Lacey, C. G., Baugh, C. M., & Frenk, C. S. 2000, *MNRAS*, 319, 168
 Colella, P., Woodward, P. R. 1984, *J. Comp. Phys.*, 54, 174
 Dahlburg, J. P., Dahlburg, R. B., Gardner, J. H., & Picone, J. M. 1990, *Phys. Fluids A*, 2, 1481
 Dalgarno, A., & McCray, R. A. 1972, *ARA&A*, 10, 375
 Dettmar, R. J. 1992, *Fund. Cosmic Phys.*, 15, 143
 Dickey, J. M., & Lockman, F. J. 1990, *ARA&A*, 28, 215
 Domgörgen, H., & Mathis, J. S. 1994, 428, 647
 Dove, J. B., & Shull, J. M. 1994, *ApJ*, 430, 222
 Draine, B. T. 1978, *ApJS*, 36, 595
 Dziourkevitch, N., Elstner, D., & Rüdiger, G. 2004, *A&A*, 423, 29
 Elmegreen, B. G. 2002, *ApJ*, 577, 206
 Elmegreen, B. G., & Scalo, J. 2004, *ARA&A*, 42, 211
 Falkovich, G. 1994, *Phys. Fluids*, 6, 1411
 Ferrière, K. M., Mac Low, M.-M., & Zweibel, E. G. 1991, *ApJ*, 375, 239
 Ferrière, K. M. 1995, *ApJ*, 441, 281
 Ferrière, K. M. 1998, *ApJ*, 503, 700
 Field, G. B., Goldsmith, D. W., & Habing, H. J. 1969, *ApJ*, 155, L49
 Frisch, U. 1995, *Turbulence. The Legacy of A. N. Kolmogorov*, Cambridge: Cambridge University Press
 Fryxell, B., Olson, K., Ricker, P., Timmes, F. X., Zingale, M. et al. 2000, *ApJS*, 131, 273
 Fujita, A., Martin, C. L., Mac Low, M.-M., & Abel, T. 2003, *ApJ*, 599, 50
 Gerritsen, J. P. E., & Icke, V. 1997, *A&A*, 325, 972
 Habing, H. J. 1968, *Bull. Astron. Inst. Netherlands*, 19, 421
 Haverkorn, M., Gaensler, B. M., McClure-Griffiths, N. M., Dickey, John M., & Green, A. J. 2004, 609, 776
 Heckman, T. M., Lehnert, M. D., Strickland, D. K., & Armus, L. 2000, *ApJS*, 129, 493
 Heckman, T. M. 2001, *ASP Conf. Proc.*, Vol. 240, ed. J. E. Hibbard et al. (ASP, San Francisco), 345
 Heiles, C. 1987, *ApJ*, 315, 555
 Heiles, C. 1990, *ApJ*, 354, 483
 Heiles, C. 2001, *ApJ*, 551, L105
 Heiles, C., & Troland, T. H. 2003, *ApJ*, 586, 1067
 Heiles, C., & Troland, T. H. 2005, *ApJ*, 624, 773
 Heitsch, F., Mac Low, M.-M., & Klessen, R. S. 2001, *ApJ*, 547, 280 (HMK01)
 Hernquist, L., & Mihos, J. C. 1995, *ApJ*, 448, 41
 Hollenbach, D., & McKee, C. F. 1979, *ApJS*, 41, 555
 Joung, M. K. R., & Mac Low, M.-M. 2005, in preparation (Paper II)
 Katz, N. 1992, *ApJ*, 391, 502
 Kennicutt, R. C., Jr., Edgar, B. K., & Hodge, P. W. 1988, *ApJ*, 337, 761
 Kim, J., Balsara, D., & Mac Low, M.-M. 2001, *J. Kor. Astron. Soc.*, 34, 333
 Kleiner, S. C., & Dickman, R. L. 1984, *ApJ*, 286, 255
 Klessen, R. S. 1998, Ph.D. thesis, Max-Planck-Institut für Astronomie, Heidelberg

- Klessen, R. S., Heitsch, F., & Mac Low, M.-M. 2000, *ApJ*, 535, 887 (KHM00)
- Korpi, M. J., Brandenburg, A., Shukorov, A., Tuominen, I., & Nordlund, Å. 1999, *ApJ*, 514, L99
- Koyama, H., & Inutsuka, S. 2004, *ApJ*, 602, L25
- Kraichnan, R. H. 1967, *Phys. Fluids* 10, 1417
- Kritsuk, A. G., Norman, M. L., & Padoan, P. 2004 (*astro-ph/0411626*)
- Krumholz, M., & McKee, C. F. 2005, *ApJ*, 630, 250
- Kuijken, K., & Gilmore, G. 1989, *MNRAS*, 239, 605
- Larson, R. B. 1981, *MNRAS*, 194, 809
- Lazarian, A., & Esquivel, A. 2003, *ApJ*, 592, L37
- Li, Y., Klessen, R. S., & Mac Low, M.-M. 2003, *ApJ*, 592, L975
- Li, Y., Mac Low, M.-M., Klessen, R. S. 2005, submitted to *ApJ* (*astro-ph/0501022*)
- Lithwick, Y. & Goldreich, P. 2001, *ApJ*, 562, 279
- Lockman, F. J. 2002, *ApJ*, 580, L47
- Mac Low, M.-M., & McCray, R. 1988, *ApJ*, 324, 776
- Mac Low, M.-M., McCray, R., & Norman, M. L. 1989, *ApJ*, 337, 141
- Mac Low, M.-M., Klessen, R. S., Burkert, A., & Smith, M. D. 1998, *Phys. Rev. Lett.* 80, 2754
- Mac Low, M.-M. 1999, *ApJ*, 524, 169
- Mac Low, M.-M., & Ossenkopf, V. 2000, *A&A*, 353, 339
- Mac Low, M.-M., & Klessen, R. S. 2004, *Rev. Mod. Phys.*, 76, 125
- Mac Low, M.-M., Balsara, D. S., Kim, J., & Avillez, M. A. 2005, *ApJ*, 626, 864
- McCray, R., & Snow, T. P., Jr. 1979, *ARA&A*, 17, 213
- McKee, C. F., & Ostriker, J. P. 1977, *ApJ*, 218, 148
- McKee, C. F. 1990, *The Evolution of the Interstellar Medium*, ASP Conf. Ser. 12, ed. L. Blitz (ASP, San Francisco), 55
- McKee, C. F., & Williams, J. P. 1997, *ApJ*, 476, 144
- Miller, G. E., & Scalo, J. M. 1979, *ApJS*, 41, 513
- Navarro, J. F., & White, S. D. M. 1993, *MNRAS*, 265, 271
- Norman, C. A., & Ferrara, A. 1996, *ApJ*, 467, 280
- Ossenkopf, V., & Mac Low, M.-M. 2002, *A&A*, 390, 307
- Ostriker, J. P., & McKee, C. F. 1988, *Rev. Mod. Phys.*, 60, 1
- Padoan, P., & Nordlund, Å. 1999, *ApJ*, 526, 279
- Padoan, P., Jones, B. J. T., & Nordlund, Å. 1997, *ApJ*, 474, 730
- Padoan, P., Nordlund, Å., & Jones, B. J. T. 1997, *MNRAS*, 299, 145
- Padoan, P., Boldyrev, S., Langer, W., & Nordlund, Å. 2003, *ApJ*, 583, 308
- Parravano, A., Hollenbach, D. J., & McKee, C. F. 2003, *ApJ*, 584, 797
- Passot, T., Pouquet, A., & Woodward, P. R. 1988, *A&A*, 197, 228
- Passot, T., & Vázquez-Semadeni, E. 1998, *Phys. Rev. E*, 58, 4501
- Pettini, M., Shapley, A. E., Steidel, C. C. et al. 2001, *ApJ*, 554, 981
- Pettini, M., Rix, S. A., Steidel, C. C. et al. 2002, *ApJ*, 569, 742
- Piontek, R. A., & Ostriker, E. C. 2005, *ApJ*, 629, 849
- Porter, D. H., Pouquet, A., & Woodward, P. R. 1992, *Phys. Rev. Lett.* 68, 3156
- Porter, D. H., Woodward, P. R., & Pouquet, A. 1998, *Phys. Fluid*, 10, 237
- Press, W. H., Teukolsky, S. A., Vetterling, W. T., & Flannery, B. P. 1992, *Numerical Recipes in FORTRAN: The Art of Scientific Computing*, Cambridge: Cambridge University Press
- Reynolds, R. J. 1991, *The Interstellar Disk-Halo Connection in Galaxies*, IAU Symp. No. 144, ed. H. Bloemen (Kluwer, Dordrecht), 67
- Rosen, A., Bregman, J. N., & Norman, M. L. 1993, *ApJ*, 413, 137
- Rosen, A., & Bregman, J. N. 1995, *ApJ*, 440, 634
- Sasao, T. 1973, *Pub. Astron. Soc. Japan*, 25, 1
- Scalo, J., Vázquez-Semadeni, E., Chappell, D., & Passot, T. 1998, 504, 835
- Sellwood, J. A. & Balbus, S. A. 1999, *ApJ*, 511, 660
- Shapiro, P. R., & Field, G. B. 1976, *ApJ*, 205, 762
- Shapley, A. E., Steidel, C. C., Pettini, M., & Adelberger, K. L. 2003, *ApJ*, 588, 65
- She, Z., & Leveque, E. 1994, *Phys. Rev. Lett.* 72, 336
- She, Z., & Waymire, E. C. 1995, *Phys. Rev. Lett.*, 74, 262
- Shull, J. M., & Saken, J. M. 1995, *ApJ*, 444, 663
- Slavin, J. D., & Cox, D. P. 1993, *ApJ*, 417, 187
- Slyz, A. D., Devriendt, J. E. G., Bryan, G., & Silk, J. 2005, *MNRAS*, 356, 737
- Somerville, R. S., & Primack, J. R. 1999, *MNRAS*, 310, 1087
- Spaans, M., & Norman, C. 1997, *ApJ*, 483, 87
- Stone, J. M., Ostriker, E. C., & Gammie, C. F. 1998, *ApJ*, 508, L99
- Strickland, D., & Stevens, I. 2000, *MNRAS*, 314, 511
- Stutzki, J., Bensch, F., Heithausen, A., Ossenkopf, V., & Zielinsky, M. 1998, *A&A*, 336, 697
- Sutherland, R. S., & Dopita, M. A. 1993, 88, 253
- Tammann, G. A., Löffler, W., & Schröder, A. 1994, *ApJS*, 92, 487
- Thacker, R. J., & Couchman, H. M. P. 2001, *ApJ*, 555, L17
- Toomre, A. 1964, *ApJ*, 139, 1217
- Vázquez-Semadeni, E., & Gazol, A. 1995, *A&A*, 303, 204
- Vázquez-Semadeni, E., Passot, T., & Pouquet, A. 1996, *ApJ*, 473, 881
- Vázquez-Semadeni, E., Gazol, A., & Scalo, J. 2000, *ApJ*, 540, 271
- Vázquez-Semadeni, E., Kim, J., & Ballesteros-Paredes, J. 2005, *ApJ*, 630, L49
- Wada, K., & Norman, C. A. 2001, *ApJ*, 547, 172
- Wakker, B. P. 2001, *ApJS*, 136, 463
- Wood, K., Mathis, J. S., & Ercolano, B. 2004, *MNRAS*, 348, 1337
- Wolfire, M. G., Hollenbach, D., McKee, C. F., Tielens, A. G. G. M., & Bakes, E. L. O. 1995, *ApJ*, 443, 152
- Wolfire, M. G., McKee, C. F., Hollenbach, D., & Tielens, A. G. G. M. 2003, 587, 278
- Zuckerman, B., & Palmer, P. 1974, *ARA&A*, 12, 279